HSR (LONDON),
HOUGHTON STREET REVIEW JOURNAL
ISSN: 2058-5519|Impact factor-15.9
http://houghtonstreetreview.com/index.php/hsr

CHANNEL DEFORMATION CAUSED BY THE INITIAL FLOW AT A CHANNEL BEND

Karshi State Technical University, Associate Professor
A.N. Isakov,
Assistants **Z.X. Sherboyev**
doi:https://doi.org/10.5281/zenodo.23256124

Abstract: At present, the approach to determining equilibrium channel topography is based on the works of Struiksma, Shimizu and Itakura, Nelson and Smith, and others. The flow field is first calculated for the initial (new) channel (in many studies, this is obtained using a steady-state hydrodynamic model) and is then provided as input data to the sediment transport model. This model calculates the erosion–accretion zones that develop under the influence of the flow over a specified short time interval, Δt.

Keywords: Deformed channel, Secondary flow circulation, Sediment transport models, Numerical schemes used, Channel planform, Discharge, Particle size.

The first objective of this study is to determine whether the incoming and outgoing initial flows themselves (i.e., without invoking secondary flow circulation) in channels with small and large bend angles can produce channel erosion–accumulation zones using the hydrodynamic model developed by Silva (1995, 1999) [95; 99].

It should be emphasized that, as noted previously, the evolution of the channel-bed relief is an unsteady process. The flow field, sediment transport rates, and changes in the channel bed interact with one another, resulting in continuous changes over time.

$$c^{-2} = c_s^{-2} + c_q^{-2} \qquad (1.1)$$

Here:

- c_s^{-2} - it is a term arising from the resistance of the channel surface (channel-bed friction) and is determined by Equation (1.2) for a sinusoidal channel with a flat bed;

$$c^{-2} = \frac{1}{K}\ln\left(11h_m / k_s\right)^{-2} \qquad (1.2)$$

- c_q^{-2} - it is a term incorporating the effect of turbulence and depends on the channel geometry and the position of the point within the flow. For a rough-bed condition in a sinusoidal channel, this value is given by Equation (1.3).

$$c_q^{-2} = \alpha_q c_s^{-2} \quad \left(R/r\right)^2 - 1 \; - \; 4\left(\left(R/B\right)^2 - 1\right)^{-1} \qquad (1.3)$$

The coefficient α_p in Equation (1.3) is expected to be a function of θ_0 and B/h_m (Silva, 1995, 1999), i.e., $\alpha_p = f(\theta_0, B/h_m)$. This means that if α_p is plotted against θ_0, a family of curves is obtained, with each curve corresponding to a different B/h_m value (see Figure 1.1). So far, only two points of these curve families have been determined through laboratory experiments.

HSR (LONDON),
HOUGHTON STREET REVIEW JOURNAL
ISSN: 2058-5519|Impact factor-15.9
http://houghtonstreetreview.com/index.php/hsr

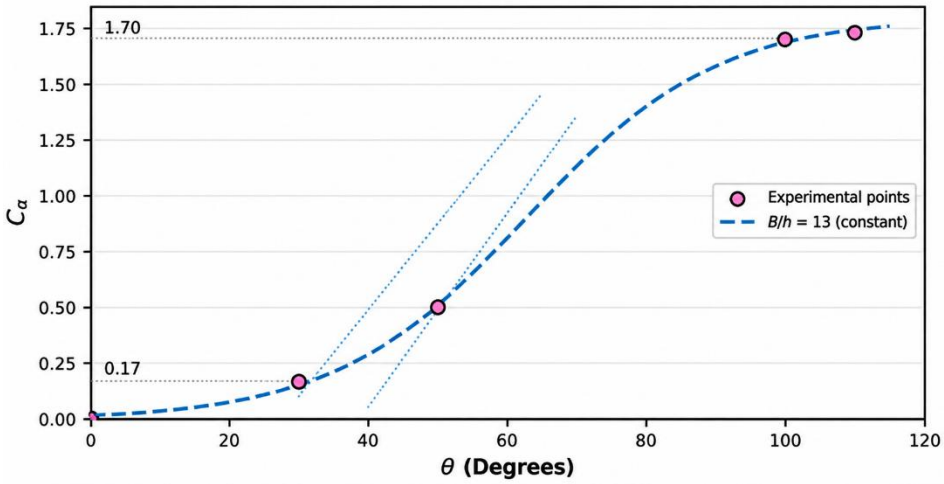


Figure 1.1. Expected variation of the coefficient α_p with θ_0 and B/h_m.

Initial flows were measured in two sinusoidal channels having bend angles of 30° and 110°. The experimental conditions are given in Table 1.1. Initial flows calculated using the hydrodynamic model are shown in Figures 1.2 and 1.5a.

The αp values that produced the best experimental results:

1.1-jadval

Field									
No.	Bend angle	Q		Soil particle diameter (D mm)	α_p	h	B	i	B/h
1	110°	1,8	5,01	2,2	1,7	0,81	7,8	0,0046	9,6
2		2,0	5,63	2,2	1,7	0,82	8,5	0,0046	10,4
3		1,8	5,87	2,2	1,7	1,39	7,0	0,0046	5,0
4		1,5	3,60	2,2	1,7	0,93	5,7	0,0046	6,2
5		1,87	3,96	2,2	1,7	0,68	7,18	0,0046	10,6
1	90°	1,92	3,63	2,2	0,16	0,69	6,64	0,0046	9,6
2		2,14	4,10	2,2	0,16	0,7	7,26	0,0046	10,4
3		1,93	4,24	2,2	0,16	1,18	5,95	0,0046	5,0
4		1,61	2,58	2,2	0,16	0,79	4,85	0,0046	6,1
5		2	2,87	2,2	0,16	0,58	6,11	0,0046	10,5
1	70°	2,04	2,84	2,2	0,17	0,57	6,12	0,0046	10,7
2		2,27	3,21	2,2	0,17	0,58	6,69	0,0046	11,5
3		2,05	3,42	2,2	0,17	0,97	5,47	0,0046	5,6
4		1,71	2,70	2,2	0,17	0,65	5,46	0,0046	8,4

HSR (LONDON),
HOUGHTON STREET REVIEW JOURNAL
ISSN: 2058-5519|Impact factor-15.9
http://houghtonstreetreview.com/index.php/hsr

5		2,13	2,24	2,2	0,17	0,48	5,62	0,0046	11,7
1		2,16	2,20	2,2	0,17	0,47	5,63	0,0046	12,0
2		2,4	2,50	2,2	0,17	0,48	6,16	0,0046	12,8
3	50°	2,17	2,74	2,2	0,17	0,8	5,03	0,0046	6,3
4		1,81	1,63	2,2	0,17	0,54	4,1	0,0046	7,6
5		2,26	1,74	2,2	0,17	0,4	5,16	0,0046	12,9
1		2,29	1,68	2,2	0,17	0,38	5,18	0,0046	13,6
2		2,55	1,91	2,2	0,17	0,39	5,67	0,0046	14,5
3	30°	2,3	2,16	2,2	0,17	0,65	4,63	0,0046	7,1
4		1,92	1,27	2,2	0,17	0,44	3,77	0,0046	8,6
5		2,4	1,35	2,2	0,17	0,33	4,75	0,0046	14,4

Silva (1995) showed that these calculated flows are very close to the measured results. When $\theta_0 = 30°$, the flow enters the channel, whereas when $\theta_0 = 110°$, the flow leaves the channel. The channel deformations calculated by the author using the sediment transport model at the channel bend are presented in Figures 1.2 and 1.5, respectively.

The calculated "channel deformations" agree with the experimental results; that is, most zones of aggradation, degradation, and transition correspond to the experimental results for $\theta_0 = 30°$ and $\theta_0 = 110°$.

Initial flows and channel topography were also calculated using the hydrodynamic model for 50°, 70°, and 90° channels (although these initial flows were not investigated by Silva (1995)). The corresponding α_p values are:

- • $\theta_0 = 50°$: $\alpha_p = 0.17$, 1.12, and 1.6
- • $\theta_0 = 70°$ and 90°: $\alpha_p = 1.2$ and 1.6

It should be noted that the predicted α_p values for $\theta_0 = 50°$ in Figure 1.1 (for example, $\alpha_p = 1.2$ and 1.6) did not agree with the experimental values. Under the conditions of Silva (1995), $\alpha_p = 1.0$ was found to be the most appropriate value during the experiments conducted in the 50° channel. The flow field for the 50° channel with $\alpha_p = 1.0$ is shown. Subsequent analysis established that $\alpha_p = 0.17$ is the best-fitting value for the 30° channel. Figures 1.8, 1.11, and 1.14 show channel deformation for the 50°, 70°, and 90° channels, respectively. Considered together with Figures 1.2 and 1.5, these results show how the "upstream migration" of erosion–deposition zones along the channel depends on θ_0.

It should be noted that although the maximum positive or negative channel-deformation value is the same (for example, $|\partial z/\partial t|_{max} \approx 0.1$ m/hour), the time required to reach this maximum changes with θ_0. Figure 1.17 shows the dependence of this time on θ_0. Channel deformation occurs most rapidly in channels with $\theta_0 = 50°$, 70°, and 90°. This is not surprising because at $\theta_0 \approx 70°$ the flow has the strongest divergence, which is expressed by the maximum of $|\partial z/\partial t|_{max}$ on the inner curve shown in Figure 1.18.

The distribution of shear stress (τ) across sections of the 30% channel-bend portion was analyzed in Figure 1.3. The results show a non-uniform distribution of shear stress along the channel. The minimum value was observed in Section 1 ($\tau = 0.38$ Pa), while the maximum value was observed in Section 9 ($\tau = 0.92$ Pa). Shear stress increased gradually between Sections 1 and 9 and then showed

HSR (LONDON),
HOUGHTON STREET REVIEW JOURNAL
ISSN: 2058-5519|Impact factor-15.9
http://houghtonstreetreview.com/index.php/hsr

a decreasing trend after Section 9 due to reduced flow energy and increased hydraulic resistance. This pattern is important for assessing channel-bed deformation, erosion, and sediment-transport processes.

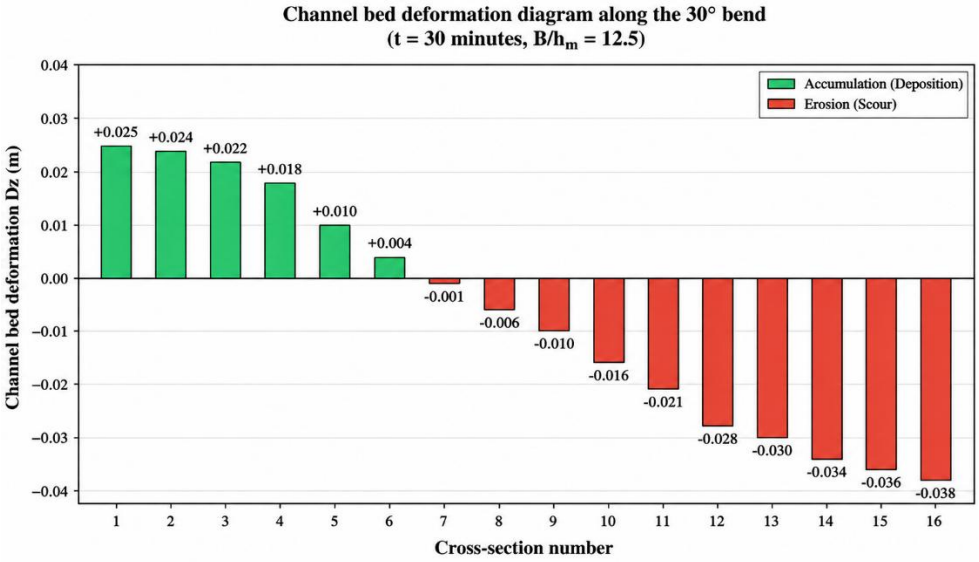


Figure 1.2. Channel-bed deformation diagram along the 30° bend of the experimental channel at B/h = 12.5.

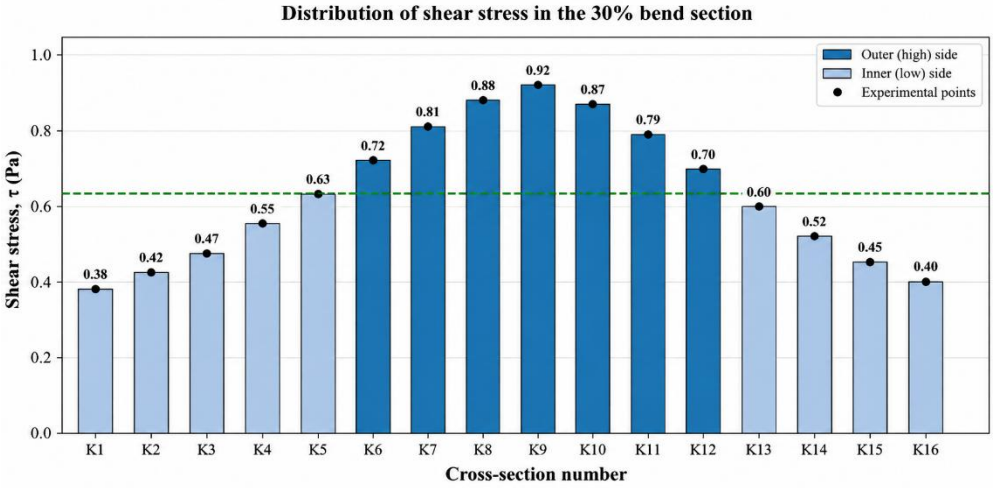


Figure 1.3. Shear stress distribution graph along the 30° channel bend at B/h = 12.5.

HSR (LONDON),
HOUGHTON STREET REVIEW JOURNAL
ISSN: 2058-5519|Impact factor-15.9
http://houghtonstreetreview.com/index.php/hsr

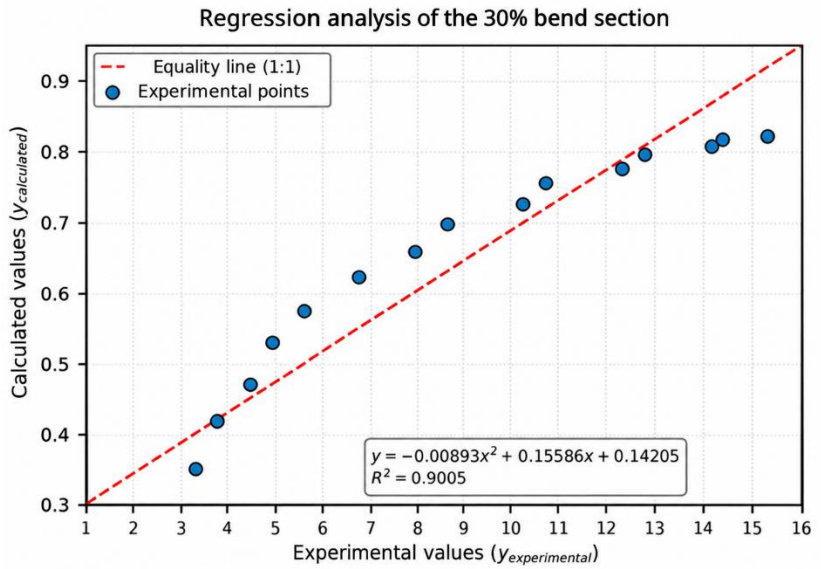


Figure 1.4. Regression analysis graph for the 30° channel bend at B/h = 12.5.

According to the 75-minute experimental results, Figures 1.5a–1.5b show a non-uniform distribution of channel-bed deformation by section under conditions of a 110° bend and B/h = 13. Erosion dominated at the inlet and outlet sections, while sediment accumulation dominated in the central part. The maximum erosion was −0.28 cm and the maximum accumulation was +0.30 cm. The results confirm the formation of erosion and accumulation zones as a result of secondary flow circulation and hydrodynamic effects.

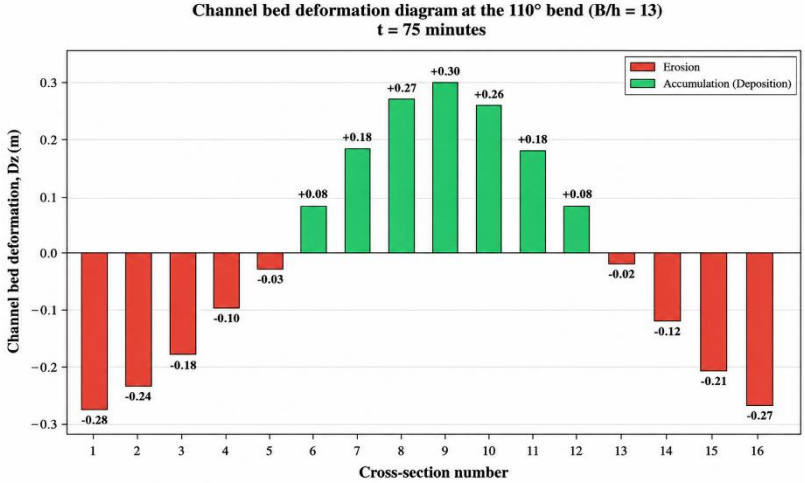


Figure 1.5 Calculated channel bed deformation for a 110° channel bend at B/h = 13 in the experiment.

HSR (LONDON),
HOUGHTON STREET REVIEW JOURNAL
ISSN: 2058-5519|Impact factor-15.9
http://houghtonstreetreview.com/index.php/hsr

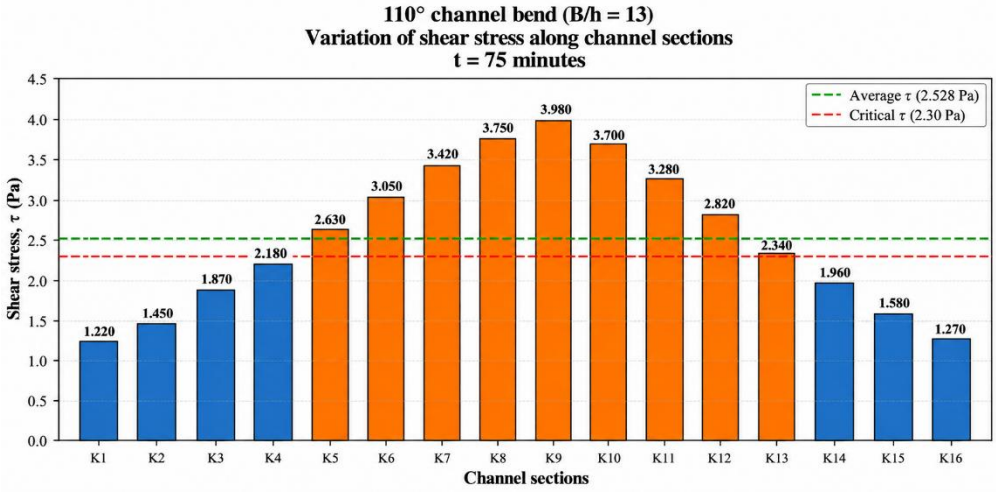


Figure 1.6. Distribution graph of shear stress calculated for a 110° channel bend at B/h = 13 in the experiment.

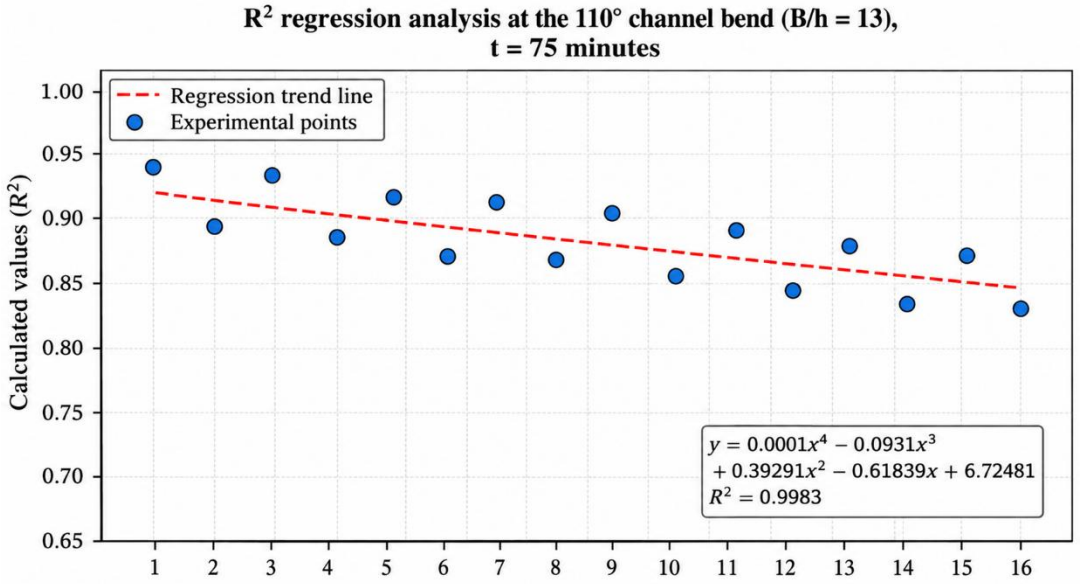


Figure 1.7. Graph of the regression values calculated for a 110° channel bend at B/h = 13 in the experiment.

HSR (LONDON),
HOUGHTON STREET REVIEW JOURNAL
ISSN: 2058-5519|Impact factor-15.9
http://houghtonstreetreview.com/index.php/hsr

Analysis of the channel-bed deformation at the 50° channel bend (B/h = 13), based on the 75-minute experimental results, showed a non-uniform distribution by section in Figure 4.8. Erosion occurred in Sections 1–3 (−0.08...−0.03 cm), while accumulation dominated in Sections 5–14, with the maximum deposition of +0.17 cm occurring in Section 9. Deformation became negative again in Sections 15–16. The trend line agrees well with the experimental results and confirms sediment accumulation in the central part and scour at the inlet and outlet sections.

According to the 75-minute experimental results, Figure 4.9 shows that shear stress exceeded 1.18 Pa along the channel sections, reached a maximum of 2.02 Pa in Section 9, and then decreased to 1.20 Pa in the final section. The trend line shows high agreement with the experimental results, confirming that shear stress reached its maximum in the central part due to increased hydraulic activity of the flow.

According to the 75-minute experimental results, Figure 4.10 shows that R^2 values changed steadily by section, increasing from 0.872 to 0.908 and reaching 0.873 in the final section. The regression curve represents the experimental data with high accuracy; $R^2 = 0.9560$ indicates a high degree of agreement between the model and experimental results. The results confirm that the regression model reliably describes changes in the channel bend.

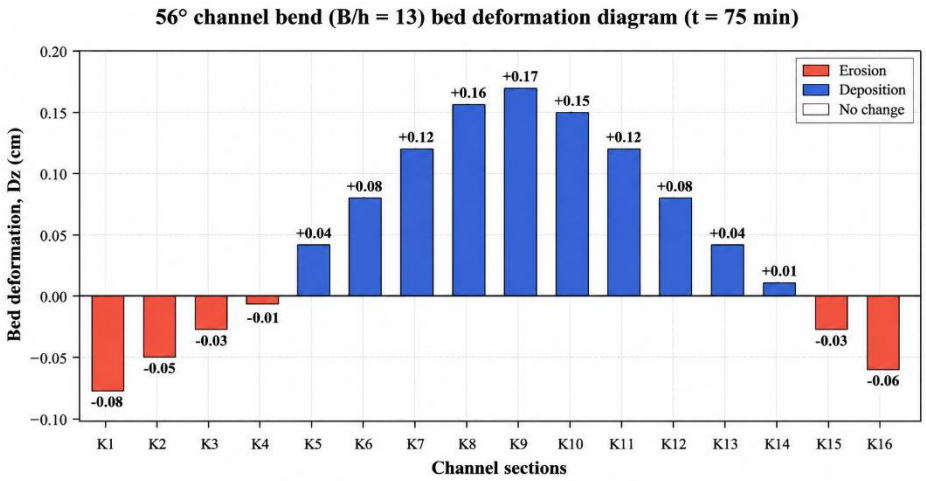
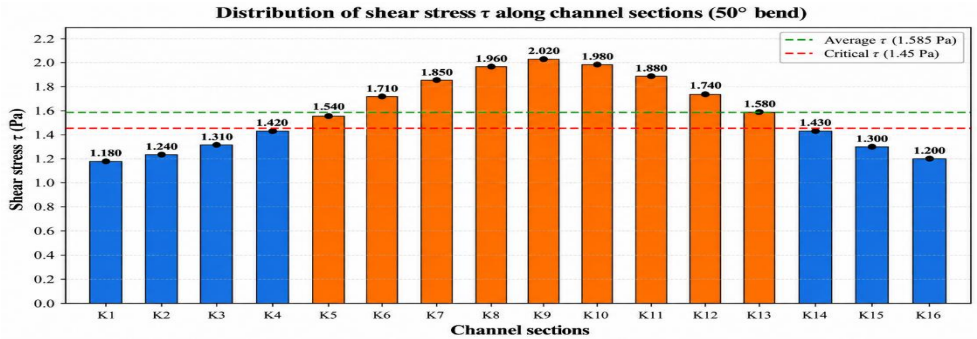


Figure 1.8. Graph of channel bed deformation at a 50° bend with B/h = 13 in the experiment.



HSR (LONDON),
HOUGHTON STREET REVIEW JOURNAL
ISSN: 2058-5519|Impact factor-15.9
http://houghtonstreetreview.com/index.php/hsr

Figure 1.9. Graph of shear stress distribution in the channel at a 50° bend with B/h = 13 in the experiment.

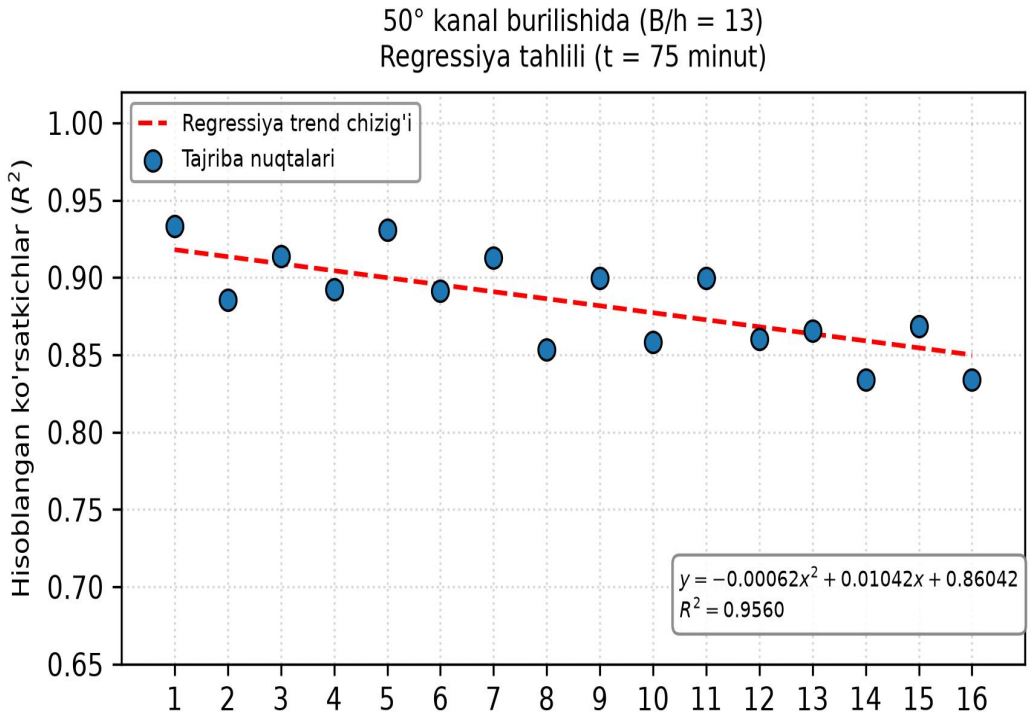


Figure 1.10. Regression analysis graph for the 50° channel bend with B/h = 13 in the experiment.

Analysis of channel-bed deformation at the 70° channel bend (B/h = 13), based on the 17-minute experimental results, showed a non-uniform distribution by section in Figure 1.11. Erosion dominated in Sections 1–8, with maximum scour of −0.33 cm in Section 5.

According to the 17-minute experimental results, Figure 1.12 shows a variable distribution of shear stress by section. The value increased from 0.12 Pa and reached 0.33 Pa in Section 5, decreased to 0.02 Pa in Section 9, and then increased again to 0.31 Pa in Section 13. In the final sections, shear stress gradually decreased and was 0.03 Pa in Section 16. The trend line agrees well with the experimental results and indicates that scour and deposition processes formed under the influence of flow redistribution and secondary flows. According to the 17-minute experimental results, Figure 1.13 shows that R^2 values changed steadily by section, exceeding 0.842, reaching 0.952 in Section 9, and equaling 0.854 in the final section. The regression model has a high level of agreement with the experimental data; the coefficient of determination $R^2 = 0.9974$ indicates that the model describes the experimental results with very high accuracy. The results confirm that the regression model reliably reflects the variation patterns for the 70° channel bend.

HSR (LONDON),
HOUGHTON STREET REVIEW JOURNAL
ISSN: 2058-5519|Impact factor-15.9
http://houghtonstreetreview.com/index.php/hsr

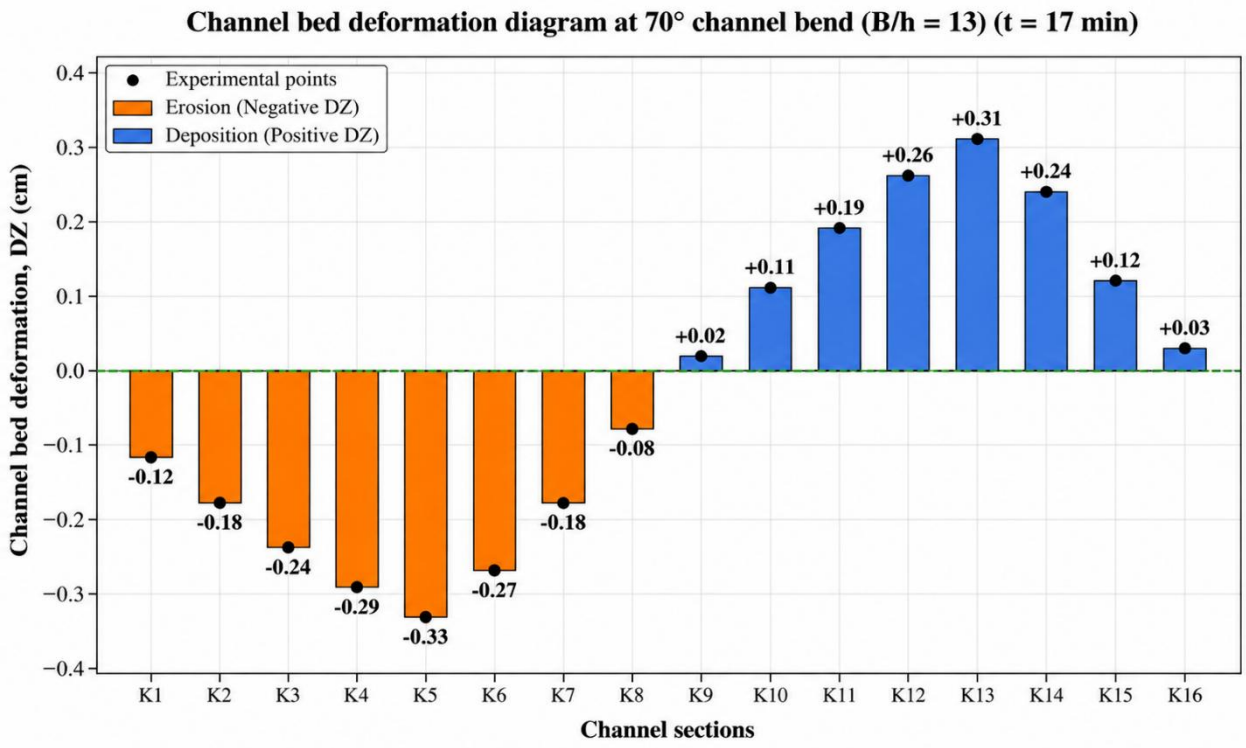


Figure 1.11. Graph of the distribution of channel bed deformation at a 70° bend with B/h = 13 in the experiment.

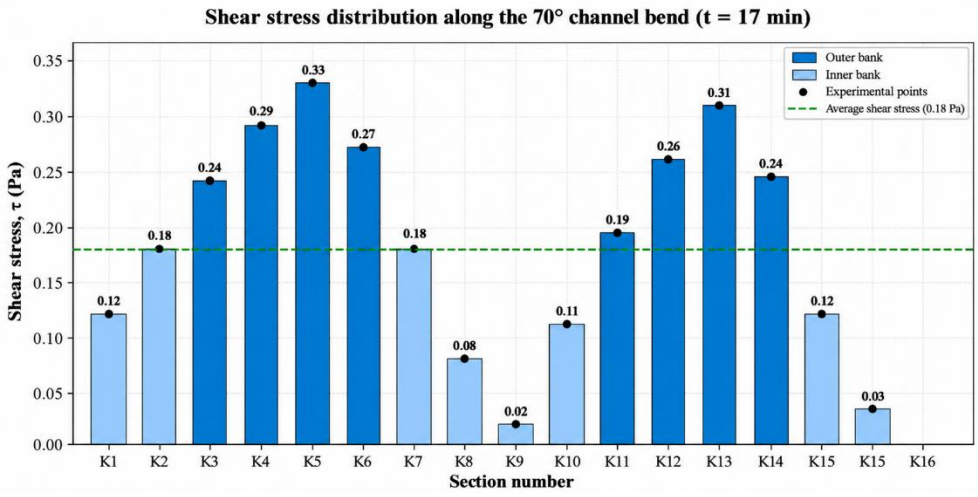


Figure 1.12. Graph of the distribution of shear stress at a 70° channel bend with B/h = 13 in the experiment.

HSR (LONDON),
HOUGHTON STREET REVIEW JOURNAL
ISSN: 2058-5519|Impact factor-15.9
http://houghtonstreetreview.com/index.php/hsr

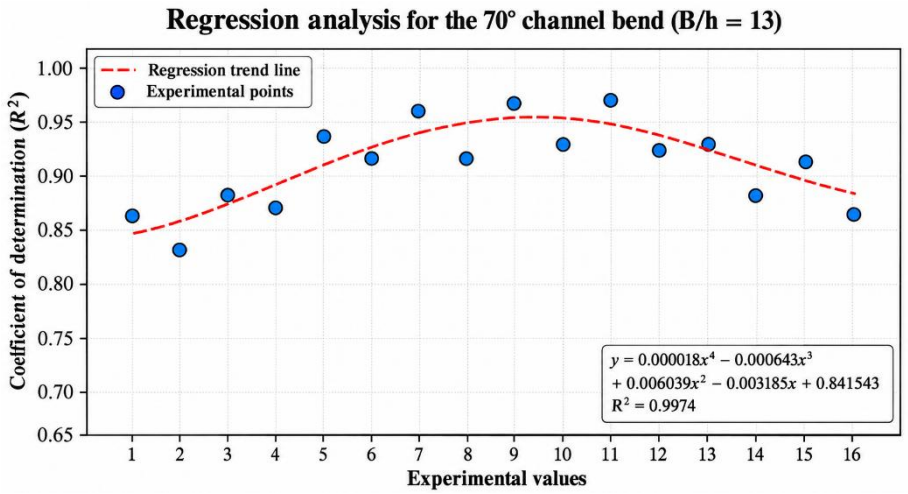
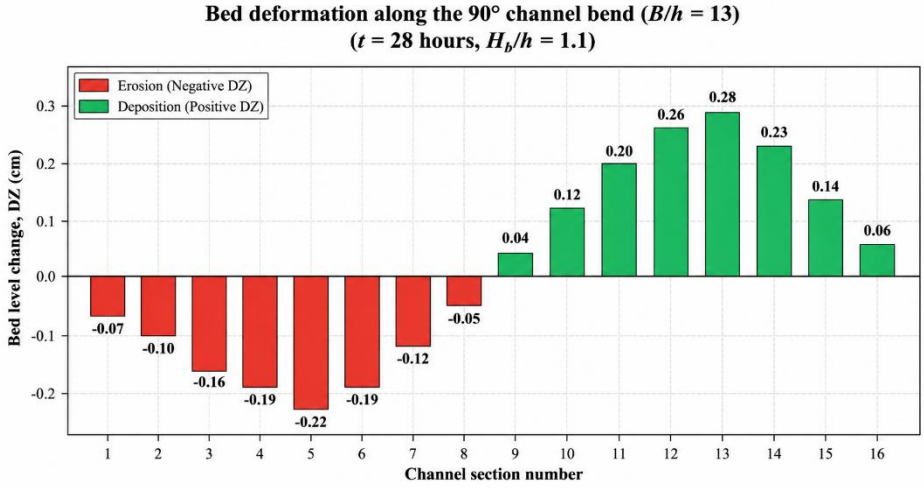


Figure 1.13. Regression analysis graph for the 70° channel bend with B/h = 13 in the experiment.

Analysis of channel-bed deformation at the 90° channel bend (B/h = 13), based on the 28-minute experimental results, showed a non-uniform distribution by section in Figure 1.14. Erosion dominated in Sections 1–8, with maximum scour of −0.30 cm in Section 5. From Section 9 onward, accumulation was observed, reaching a maximum deposition of +0.32 cm in Section 13; in Section 16 it was +0.05 cm. The results indicate that scour dominates at the inlet, while sediment accumulation dominates in the central and outlet sections of the 90° bend.

According to the 28-minute experimental results, Figure 4.15 revealed a strong inverse linear relationship between channel-bed deformation (DZ) and shear stress (τ). The regression equation is $\tau = -0.413 \cdot DZ + 0.167$, expressing a decrease in shear stress as deformation increases. Figure 4.16 confirms, with a coefficient of determination $R^2 = 0.9812$, that the model agrees highly with the experimental results. The obtained results show that the regression model can be reliably applied to assess and predict channel-bed deformation.



HSR (LONDON),
HOUGHTON STREET REVIEW JOURNAL
ISSN: 2058-5519|Impact factor-15.9
http://houghtonstreetreview.com/index.php/hsr

Figure 1.14. Diagram of channel bed scour and deposition at a 90° bend with B/h = 13 in the experiment.

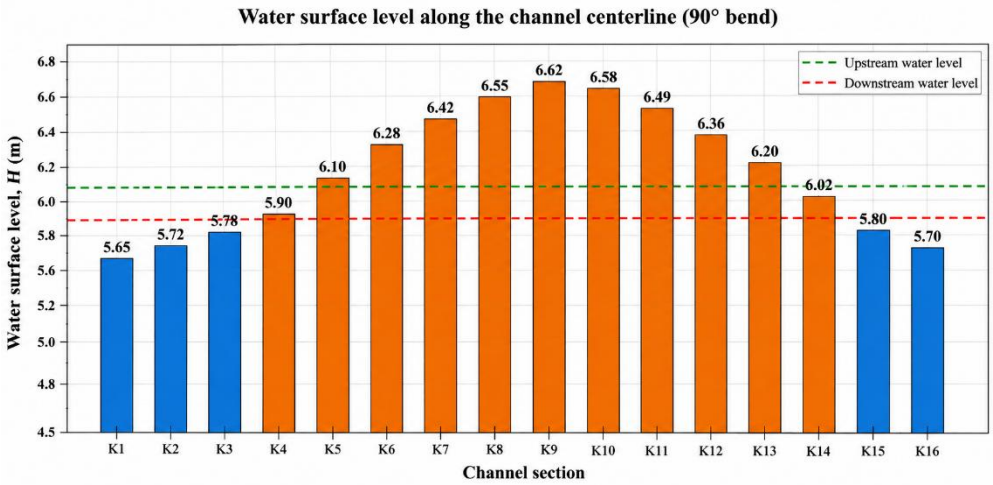


Figure 1.15. Graph of shear stress at a 90° channel bend with B/h = 13 in the experiment.

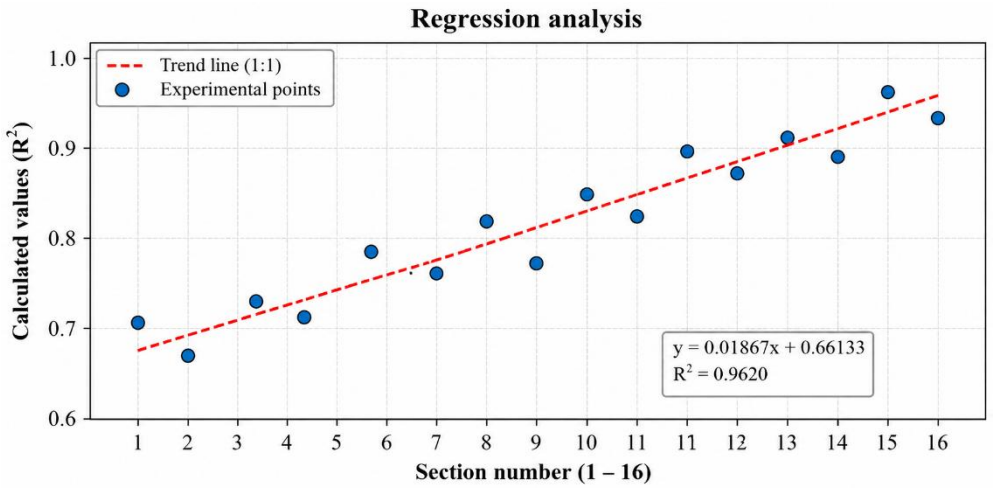


Figure 1.16. Regression analysis graph for the 90° channel bend with B/h = 13 in the experiment.

HSR (LONDON),
HOUGHTON STREET REVIEW JOURNAL
ISSN: 2058-5519|Impact factor-15.9
http://houghtonstreetreview.com/index.php/hsr

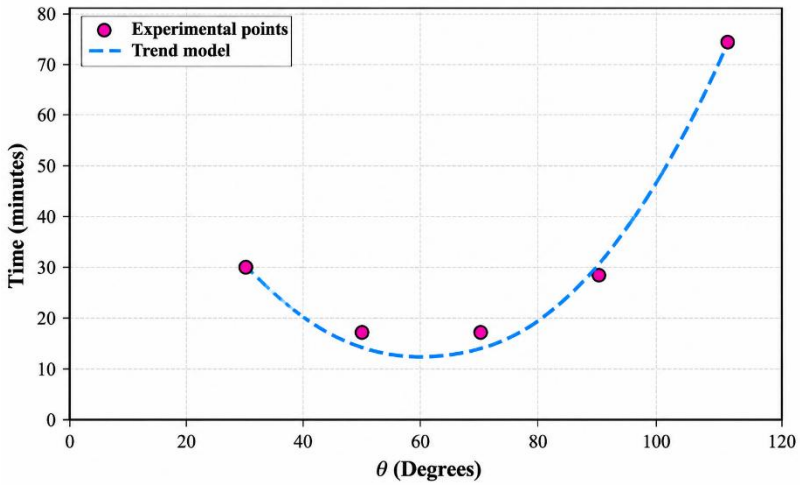


Figure 1.17. Variation in the time required for uniform deformation to develop in channels as a function of the θ_0 angle in the experiment.

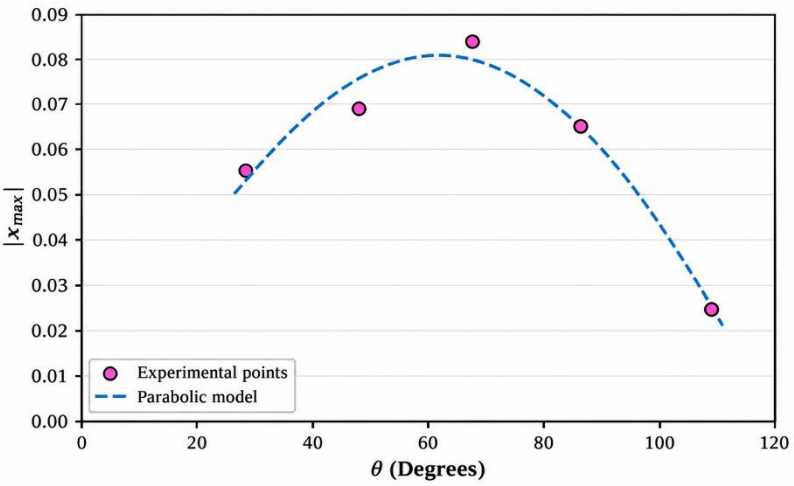


Figure 1.18. Variation of the maximum deformation value $|x_{max}|$ with respect to the θ_0 angle in the experiment.

According to the results in Figure 1.17, the effect of the channel-bend angle on the experimental duration changed according to a nonlinear relationship as the bend angle increased. The experimental duration was 30 minutes for a 30° bend, 18 and 17 minutes for 50° and 70° bends, respectively. For a 90° bend, this value increased to 28 minutes, and for a 110° bend it increased to 75 minutes. The trend line represents the results well and shows minimum duration in the 50–70° range, while maximum duration was observed for 90–110° bends due to the hydrodynamic complexity of the flow.

According to the results in Figure 1.18, the maximum scour depth varied nonlinearly with the bend angle. It was 0.055 at a 30° bend, increased for 50° and 70° bends, and reached a maximum

HSR (LONDON),
HOUGHTON STREET REVIEW JOURNAL
ISSN: 2058-5519|Impact factor-15.9
http://houghtonstreetreview.com/index.php/hsr

value of 0.084 at 70°. When the bend angle increased to 90° and 110°, the scour depth decreased to 0.065 and 0.025, respectively. The parabolic trend model agrees well with the experimental results and shows that erosion was most intense at a 70° bend, whereas at larger angles scour intensity decreased due to redistribution of the flow.

REFERENCES

1. Ciracy, C. On Secondary Flows. Proceedings of the International Association of Hydraulic Research (IAHR) Conference, September 1967, Fort Collins, Colorado.
2. Einstein, H.A., Harder, J.A. Velocity Distribution and Boundary Layer in Channel Bends. Transactions of the American Geophysical Union, 35 (1954): 114–120.
3. Francis, J.R.D., Asfari, A.F. Velocity Distribution in Wide Curved Open Channels. Hydraulic Research, 9 (1971): 73–90.
4. Friedkin, J.F. Laboratory Investigation of Meandering in Alluvial Rivers. U.S. Waterways Experiment Station, Vicksburg (1945).
5. Godfrey, R.G. Evaluation of Current Meters. U.S. Geological Survey, Research Seminar (1958).
6. Eshev, S., Isakov, A., Abdurakhmonov, A., Sherboev, Z., Yuldosheva, U., & Ramiz, A. (2025, June). Calculation of the geometric characteristics of the washing funnel. In AIP Conference Proceedings (Vol. 3286, No. 1, p. 040037). AIP Publishing LLC.
7. Duskulov, A., Isakov, A., & Jalilov, Z. (2020, July). Selection of the number of teeth of the sprockets of the soil seeder. In IOP Conference Series: Materials Science and Engineering (Vol. 883, No. 1, p. 012141). IOP Publishing.